Ocean Dynamics (2010) 60:1177–1192
DOI 10.1007/s10236-010-0320-4

Eddy-permitting simulations of the sub-polar North Atlantic: impact of the model bias on water mass properties and circulation

Jieshun Zhu · Entcho Demirov · Fred Dupont · Daniel Wright

Received: 1 February 2010 / Accepted: 14 July 2010 / Published online: 12 August 2010

Abstract Some previous studies demonstrated that model bias has a strong impact on the quality of long-term prognostic model simulations of the sub-polar North Atlantic Ocean. Relatively strong bias of water mass characteristics is observed in both eddy-permitting and eddy-resolving simulations, suggesting that an increase of model resolution does not reduce significantly the model bias. This study is an attempt to quantify the impact of model bias on the simulated water mass and circulation characteristics in an eddy-permitting model of the sub-polar ocean. This is done through comparison of eddy-permitting prognostic model simulations with the results from two other runs in which the bias is constrained by using spectral nudging. In the first run, the temperature and salinity are nudged towards climatology in the whole column. In the second run, the spectral nudging is applied in the surface 30 m layer and at depths below 560 m only. The biases of the model characteristics of the unconstrained run are similar to those reported in previous eddy-permitting and eddy-resolving studies. The salinity in the surface and intermediate waters of the Labrador Sea waters increases with respect to the climatology, which reduces the stability of the water column. The deep convection in the unconstrained run is artificially intensified and the transport in the sub-polar gyre stronger than in the observations. In particular, the transport of relatively salty and warm Irminger waters into the Labrador Sea is unrealistically high. While the water mass temperature and salinity in the run with spectral nudging in the whole column are closest to the observations, the depth of the winter convection is underestimated in the model. The water mass characteristics and water transport in the run with spectral nudging in the surface and deep layers only are close to observations and at the same time represent well the deep convection in terms of its intensity and position. The source of the bias in the prognostic model run is discussed.

Keywords The sub-polar North Atlantic · Model bias · Spectral nudging · Eddy-permitting ocean models · Water mass properties · Ocean circulation

Responsible Editor: Richard John Greatbatch

J. Zhu · E. Demirov (✉)
Memorial University of Newfoundland,
St. John's, Newfoundland, Canada
e-mail: entcho@mun.ca

F. Dupont
Dalhousie University,
Halifax, Nova Scotia, Canada

D. Wright
Bedford Institute of Oceanography,
Dartmouth, Nova Scotia, Canada

1 Introduction

The sub-polar North Atlantic (Fig. 1) is a complex physical system, which plays a key role in global climate dynamics. In the Labrador Sea, the general cyclonic circulation and strong oceanic winter heat loss create conditions for open-ocean deep convection and formation of the Labrador Sea Water (LSW) (Marshall and Schott 1999). Together with the Greenland–Scotland Overflow water which originates from mid-depths in the Nordic Seas, LSW contributes to the North Atlantic Deep Water (NADW), which acts as the lower limb of the global Meridional Overturning Circulation and has an important impact on the climate of the Earth itself. Hydrographic observations have revealed that, recently, the sub-polar North Atlantic experienced significant changes on the interannual to interdecadal time scales

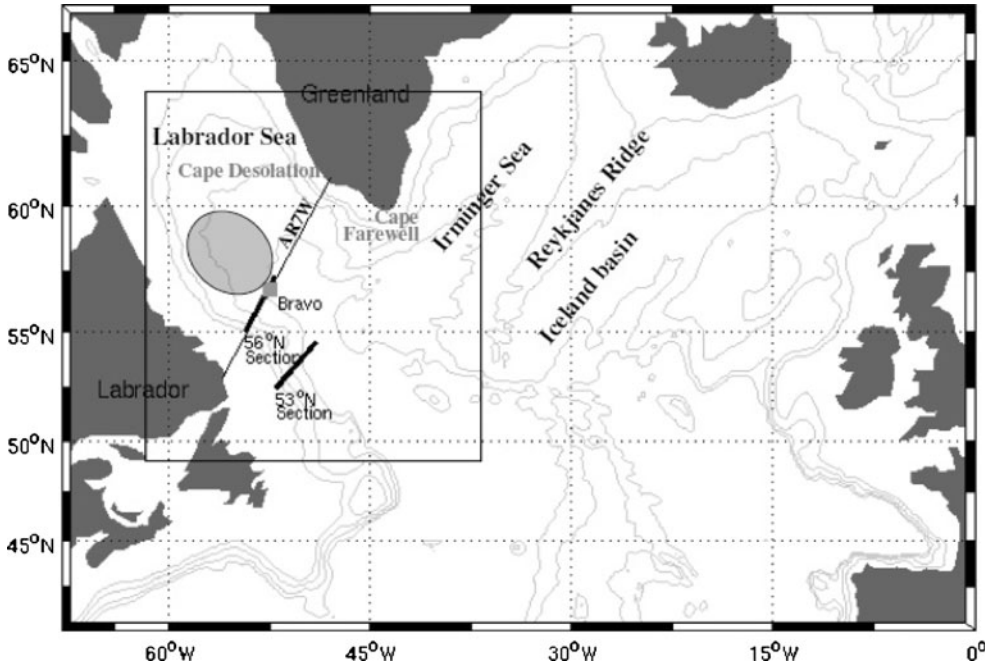

Fig. 1 Orientation map of the sub-polar North Atlantic. The isobaths are 700, 2,000, 3,000, 3,500, and 6,000 m (*light contours*). Also marked are the locations of the former OWS Bravo (*square*) and of the WOCE AR7W hydrographic section (*black line* between Hamilton Bank, Labrador, and Cape Desolation on the West Coast of Greenland). The location of the deep convection site (*shaded ellipse*) is shown after Pickart et al. (2002) based on the data of the winter of 1997. The two sections (*black lines*; namely, 53° N and 56° N sections) perpendicular to the shelf break in the Labrador Sea are where the deep Labrador currents were monitored repeatedly over the last decade (Dengler et al. 2006). The *outlined box* in the northwest Atlantic is for area average in Fig. 2

(Dickson et al. 2002; Hakkinen and Rhines 2004; Lohman et al. 2009). During the recent decade, there has been much effort in modeling the sub-polar North Atlantic Ocean. The results from the DYNAMO project (Willebrand et al. 2001), in particular, demonstrated that the bias in the eddy-permitting models of the sub-polar North Atlantic reduces the realism of the long-term simulations. More recently, Tréguier et al. (2005) presented results from comparison of simulations by several eddy-resolving models in the sub-polar North Atlantic (1/10° Parallel Ocean Program model, 1/12° Miami Isopycnic Coordinate Ocean Model, 1/6° French Atlantic model, and 1/12°Family of Linked Atlantic Ocean Model Experiments). The results from this study showed that the increased resolution in these models did not significantly reduce the bias. In particular, all four models show a large bias in water mass properties.

The aim of this article is to assess the effect of the model bias on the simulated circulation and water mass properties in the sub-polar North Atlantic. We use the spectral nudging scheme of Thompson et al. (2006) which is an effective and computationally efficient method to reduce bias in ocean models. Previously, the spectral nudging has been applied in open ocean (Lu et al. 2006; Wright et al. 2006; Stacey et al 2006), coastal (Thompson et al. 2007), and data assimilation (Liu and Thompson 2009) studies. In this work, we use the spectral nudging to reduce bias in an eddy-permitting model and compare these simulations with an unconstrained free model run.

The article is organized as follows: The numerical model and experiments designs are described in "Section 2". In "Section 3" and "Section 4", we compared the simulated water mass characteristics and water mass transport, respectively. The spatial patterns of the model drift and its causes are discussed in "Section 5". "Section 6" presents results from hindcast simulations forced with interannual forcing. "Section 7" offers conclusions.

2 The model and experiments design

The numerical model used in this study is Nucleus for European Models of the Ocean (Madec 2008) modeling system, which is a primitive equation, free surface ocean circulation code OPA9 (Madec 2008) coupled with the multilayered sea ice code LIM2 (Fichefet and Morales Maqueda 1997). The model parameters are summarized in Table 1.

2.1 Model configuration

The model domain covers the North Atlantic from 7° N to 67° N with a Mercator isotropic longitude × latitude grid

Table 1 Model parameters

Name of model	Horizontal resolution	Horizontal dimensions	Time step (s)	Max. horizontal resolution (km)	Min. hrizontal resolution (km)	Max. biharmonic viscosity (m^4/s)	Max. Laplacian diffusivity (m^2/s)
NA025	1/4°×1/4° cosØ	544×336	2,400	27.6	11.0	−1.5E+11	300

and 46 vertical levels. The horizontal resolution is 1/4° in longitude and 1/4° cosϕ in latitude. This resolution corresponds to model grid spacing of about 28 km at 7° N and 11 km at 67° N. A free-slip boundary condition is applied at land boundaries. Open boundary conditions (OBC) at the northern and southern boundaries are defined according to the formulation by Tréguier et al. (2001) and Marchesiello et al. (2001). These are radiation OBC with constrain of the long-term variability of model quantities at the open boundaries by their climatological values, which in the present study are defined from SODA data (Carton et al. 2005). Vertical grid spacing is irregular with 8 m resolution at the surface, which smoothly increases to 280 m at the bottom. The maximum model depth is 5,600 m.

The model bathymetry is derived from the 2-min resolution ETOPO2 bathymetry file of National Geophysical Data Center (US Department of Commerce et al. 2006). The bathymetry data are interpolated on the model grid by using the median method, and then two passes of Shapiro filter is applied to the topography. A few hand editing is performed, such as removing some closed seas.

Partial step (Adcroft et al. 1997) method is applied to represent topography. The energy–enstrophy conserving scheme (Arakawa and Lamb 1981), which conserves total energy for general flow and potential enstrophy for flows with no mass flux divergence, is used in momentum equations. These options were found to get the better performance in the simulations of the North Atlantic by the previous studies of Barnier et al. (2006) and Penduff et al. (2007).

The vertical mixing is parameterized by the 1.5 turbulent closure model of Gaspar et al. (1990), adapted to OPA by Blanke and Delecluse (1993). In case of static instability, a viscosity /diffusivity enhancement of 10 m^2/s is used. A Laplacian lateral isopycnal diffusion on tracers is used (300 m^2/s at 7° N and decreasing poleward proportionally to the grid size), while a horizontal biharmonic viscosity is used for momentum (-1.5×10^{11} m^4/s at 7° N and decreasing poleward as the cube of the grid size).

Initial conditions for temperature and salinity are derived from WOA05 dataset (Locarnini et al. 2006; Antonov et al. 2006) for the North Atlantic and Baltic Sea and from MEDAR dataset (Brankart and Brasseur 1998) for the Mediterranean Sea. The model is forced by surface heat, freshwater, and momentum fluxes which are computed with climatological monthly mean. The latter are derived from the NCEP/NCAR reanalysis (Kalnay et al. 1996) for the period of time from 1968 to 1996.

2.2 Numerical experiments

Three experiments are carried out in this study to examine the sensitivity of the North Atlantic sub-polar gyre simulations to the model bias. In these experiments, we use the spectral nudging approach developed by Thompson et al (2006) to suppress the model bias. This method corrects the model solution in specific frequencies and wave-number intervals. Outside these intervals, the solution is not constrained. In this study, the spectral interval of the nudging is defined in a way that it suppresses the bias in the mean and seasonal cycle of temperature and salinity in the model solution (see Appendix 1).

All three experiments use the same model configurations. The only difference between them is that spectral nudging is used in a different way. In the first experiment (EXP1), temperature and salinity on all model levels are nudged to the climatological fields; in EXP2 the upper three (28 m) and lower 20 levels (deeper than 560 m) are nudged, and no spectral nudging is applied at depths 28–560 m; in EXP3, only the upper three levels are nudged. In the last run EXP3, only temperatures and salinities in the surface layer are constrained by the spectral nudging to correct the model uncertainties due to unknown surface fluxes. Thus, this simulation is a free run where the model solution in the water column below the surface is unconstrained.

In addition, considering the existence of sea ice at high latitudes, in all experiments no nudging is applied for temperature in the surface three layers in the regions north of 50°N. The spectral nudging is always applied in all experiments in the Gulf of Cadiz for the layer from 450 to 1,500 m. Our previous simulations (not shown here) suggested that the dynamics and spreading of Mediterranean water masses into the North Atlantic Ocean are not well represented by the eddy-permitting model. By applying the spectral nudging in this region, we constrained the model temperature and salinity close to observed ones during the whole period of simulation. Similar corrections were made also in other eddy-permitting simulations (Molines et al. 2007).

EXP1 has been initialized at rest and run for 30 years. EXP2 and EXP3 were initialized from the state of the tenth year of EXP1 run and have been run for another 20 years. Figure 2 shows the time evolution of total kinetic energy, potential temperature, and salinity from the three experiments averaged over the Labrador Sea region. During the first 10 years, the variability of all three parameters in EXP1 shows oscillations with a period of about 2 years, which dissipate gradually after 10 years. During the last 10 years, the solutions in all three experiments reach the quasi-stationary state, with well-defined seasonal cycles in all three variables. The integral parameters in EXP2 and EXP1 are close during the whole period. The waters in the Labrador Sea are warmer, saltier, and have higher kinetic energy in EXP3 than in other two runs. In the following sections, our discussions about water mass characteristics and transports are mainly based on the last 5 years of each experiment.

3 Water mass characteristics in the subpolar North Atlantic

3.1 Mean hydrography along the WOCE AR7W section

Here we compare the mean thermohaline properties from the three experiments on the section between Hamilton Bank, Labrador, and Cape Desolation on the West Coast of Greenland (WOCE AR7W). Numerous hydrographic surveys have been carried during the WOCE experiment along this section. The temperature and salinity distribution along the AR7W represents the structure of the main water masses of the Labrador Sea, their variability and their connection to the general circulation in the region. On the Greenland side, the West Greenland Current flows northwards with cold and fresh water near the surface. Below this current, the relatively warm and salty Irminger water flows northwards. The cold Labrador Current flows southward in the eastern part of the Labrador Sea. The Deep Labrador Current extends down to the bottom. The mid-depths (1,000–2,000 m) of the basin's interior are filled with low-stratified, convection-formed Labrador Sea.

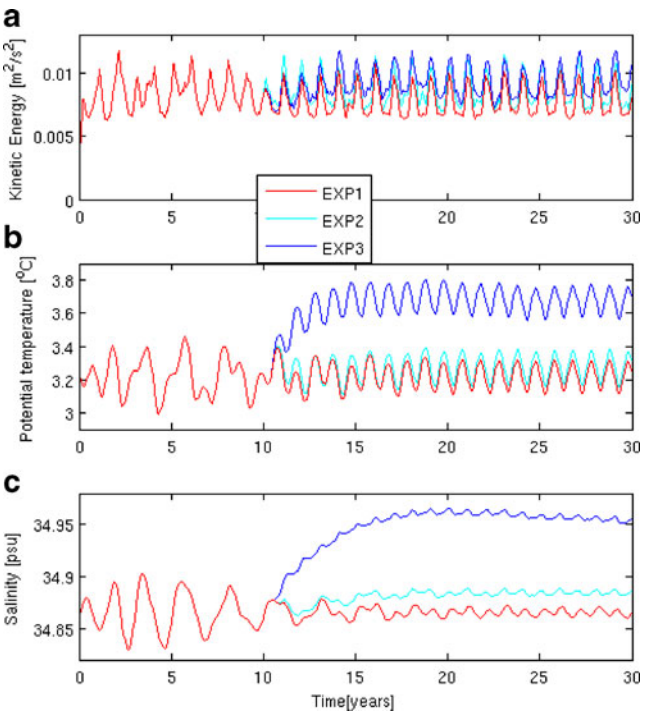

Fig. 2 The time evolution of total kinetic energy (m^2/s^2), potential temperature (°C), and salinity (psu) from the three experiments averaged over the Labrador Sea region outlined in Fig.1 as a box

The potential temperature and salinity from the WOA05 data set are shown in Figs. 3a and 4a, respectively. Figures 3b and 4b present the bias (computed as model minus climatology) of potential temperature and salinity in EXP1 relative to WOA05. The mean thermohaline properties of EXP1 are in good agreement with WOA05 except for the regions along the eastern and western boundaries. The comparison in these regions includes some level of uncertainty since the WOA05 dataset has the resolution of 1° and does not resolve smaller-scale phenomenon related to the near coastal dynamics. The mean temperature and salinity at the depths below about 1,500 m in EXP2 (Figs. 3c and 4c) are similar to that in EXP1. These two data sets show some differences mostly near the surface and at intermediate depths. In particular, the intermediate layer water in EXP2 has weaker stratification compared to EXP1. The bias in mean temperature and salinity is strongest in the EXP3 (Figs. 3d and 4d). The water masses in the Labrador Sea have become unrealistically warmer and saltier, including both boundary currents and the deep water. Along most of the section, the temperature and salinity increases by about 0.5–1°C and 0.1–0.2 psu. The water mass characteristics become unrealistic in EXP3 after 20 years of simulations. This was also observed in the previous studies (Willebrand et al. 2001; Tréguier et al. 2005). In the following sections, we will study the impact which the model bias has on dynamics and circulations of the sub-polar area.

3.2 Temperature and salinity at mid-depth

Figures 5 and 6 present the potential temperature and salinity at middle depth (648 m) from WOA05 dataset and for the three experiments. The simulations in the EXP1 are closest to WOA05 climatology. The major differences are observed along the coasts of the Irminger Sea and the Labrador Sea where the boundary current dynamics effect introduces a relatively small-scale variability in the model

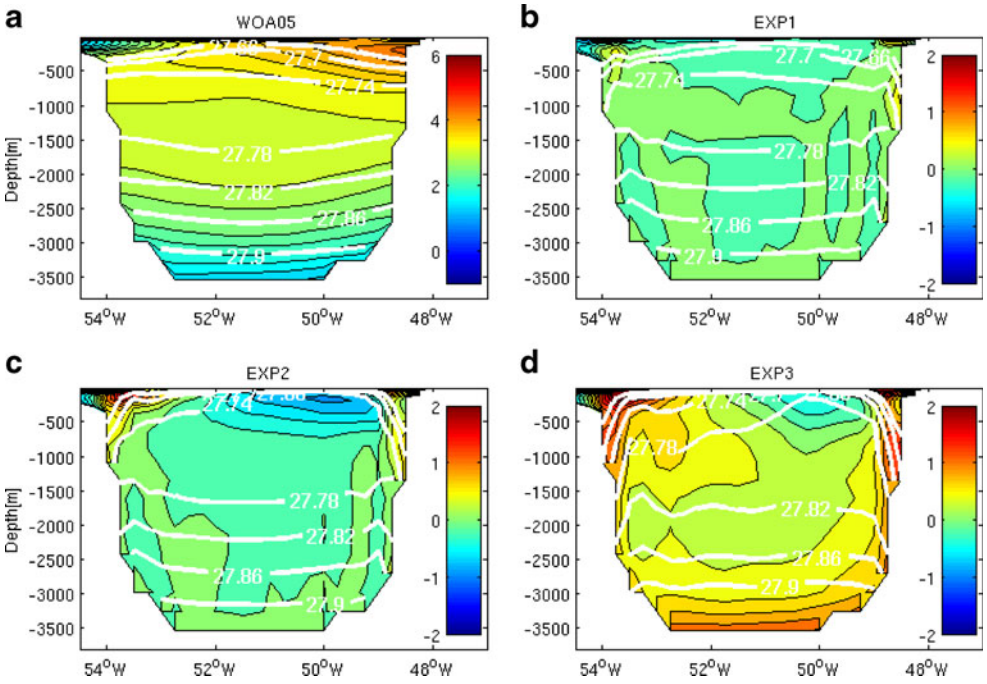

Fig. 3 **a** The distribution of potential temperature across the Labrador Sea along the WOCE AR7W section from WOA05. **b** The bias of potential temperature in EXP1 relative to WOA05 (**a**). **c** The bias of potential temperature in EXP2. **d** The bias of potential temperature in EXP3. Contour interval is 0.2° C. The *contours in white* are potential densities with reference to surface (kg $^{-3}$)

comparing with WOA05 climatology. The model bias has a larger impact on the distribution of temperature and salinity in EXP2 and EXP3. In "Section 4", we will see that the bias is consistent with the difference between the circulation patterns in these two experiments.

Temperature and salinity in the three experiments also differ over the Reykjanes Ridge. In EXP1 and EXP2, the two fields are very close to the WOA05 climatology in the open ocean. Near the shelf/slope, the model flow slightly modifies the temperature and salinity distribution, but the distribution of the two fields still closely follows the data. In contrast with WOA05 climatology, the contours of the temperature and salinities in EXP3 tightly follow the bathymetry over the Reykjanes Ridge. This distribution is typical for model simulations of this sub-polar region without constrain of subsurface temperature and salinity (see Treguier et al. 2005). In this experiment, however, there is an artificial strong extension of the sub-polar gyre eastward. The front between the sub-polar gyre and the North Atlantic current shifts eastward, which results in

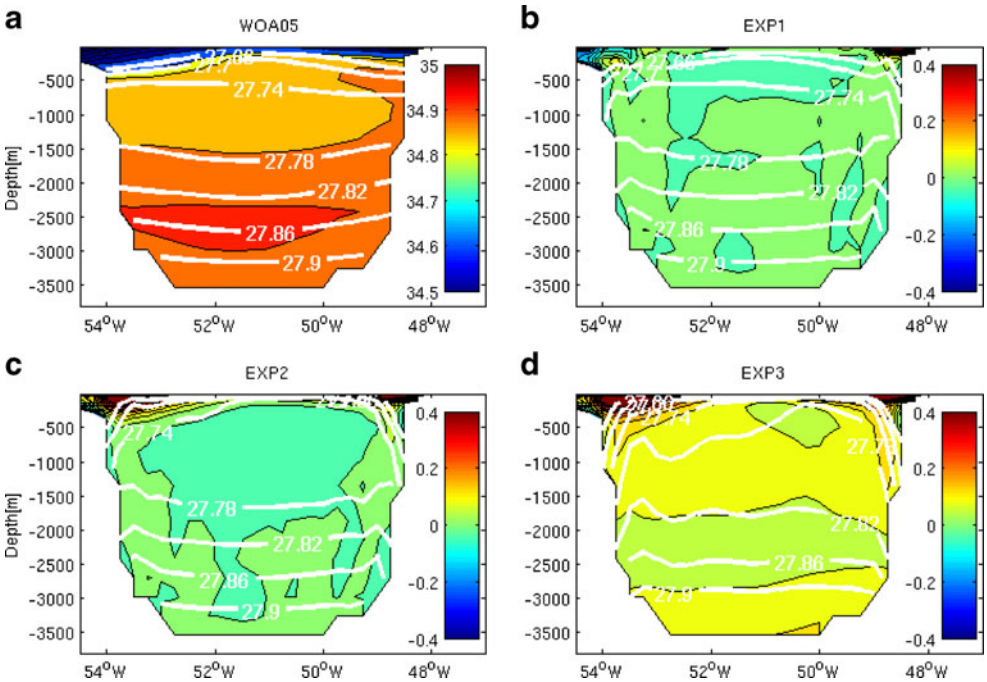

Fig. 4 **a**–**d** As in Fig. 3 but for salinity (unit, psu). The *contours in white* are potential densities with reference to surface (kg m^{-3}). In the upper layers of **a**, the salinity <34.5 is shown in *dark blue*

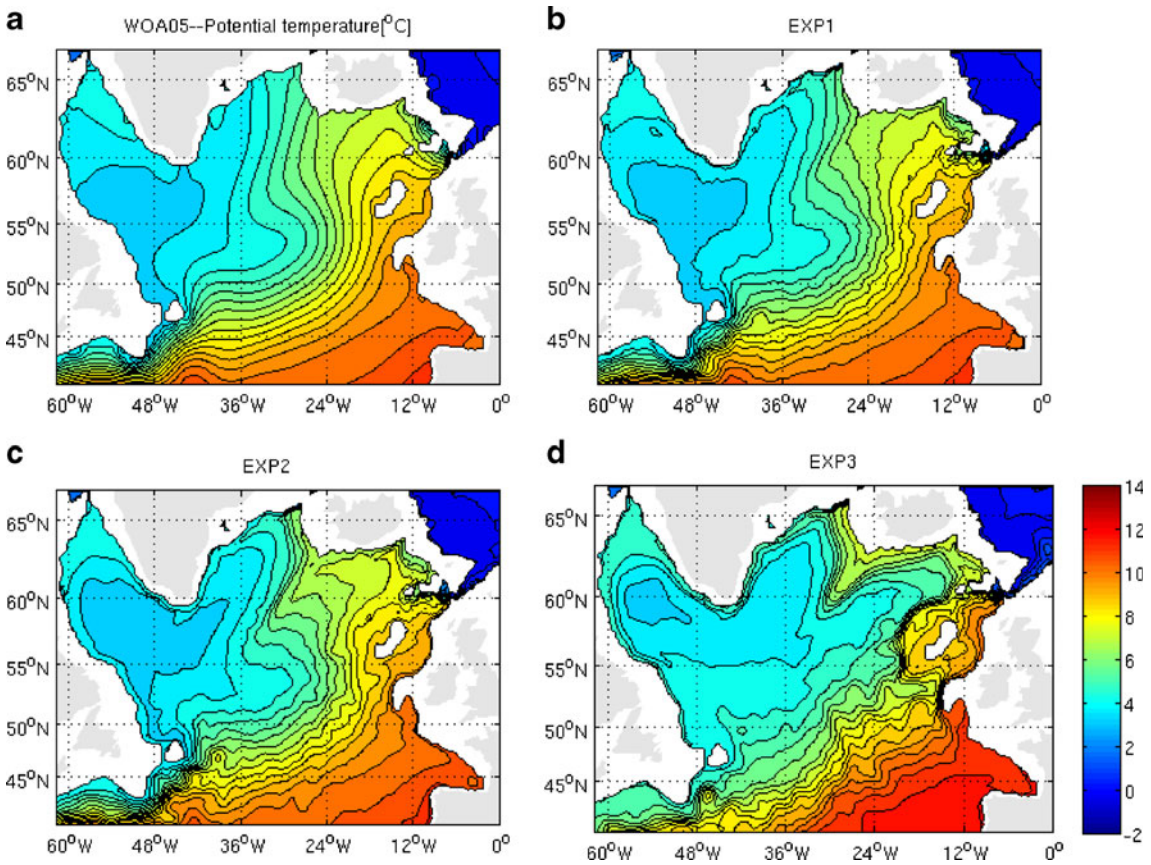

Fig. 5 Potential temperature at intermediate depth (648 m) from **a** WOA05, **b** EXP1, **c** EXP2, and **d** EXP3. Contour interval is 0.5°C

unrealistic temperature and salinity fields in the deep part of this region.

3.3 Temperature and salinity profiles

The mean vertical temperature and salinity profiles shown in Fig. 7 are calculated in three boxes in the inner Labrador Sea, the inner Irminger Sea, and Iceland Basin, as indicated in Fig. 6a. Each vertical profile shows four curves which represent the WOA05 data and the three experiments. In all three sites, the temperature and salinity profiles from EXP1 are close to the WOA05 (Fig. 7). In the EXP3, the profiles show some similar biases as in the previous study of Treguier et al. (2005). In particular, in the Labrador Sea and Irminger Sea, the water columns below 1,000 m are about 0.1 psu saltier than WOA05 and about 1–1.5°C warmer. In the Labrador Sea and Irminger Sea, not only deep layers but also the surface waters are saltier than observations. Treguier et al. (2005) explains this bias as a result of: (1) lack of fresh water input from sea ice melting and river runoff, (2) unrealistic representation of the East Greenland Coastal Current, and (3) unrealistic transport of the salty water above or around the Reykjanes Ridge. Myers and Deacu (2004) explain the salinity bias with the too strong import of high-salinity water from the North Atlantic current and the enhanced export of Labrador Sea Water to the Irminger Sea. Our results discussed in "Section 4" also suggest that the enhanced water transport of salty Atlantic water around Reykjanes Ridge can contribute to the "salinization" bias in Labrador Sea.

3.4 Deep convection

Deep convection in the Labrador Sea depends on the properties of the circulation and the water mass (Marshall and Schott 1999). In this section, we compare the simulated deep convection in the three experiments. Figure 8a–c show the mixed layer depths (MLD) in Labrador Sea in late March for the three experiments. The MLD is defined as the depth where potential density exceeds the surface density by 0.01 kg/m^3. The maximums of the mixed layer depth in Labrador Sea are less than 2,500 m in the three experiments.

The MLD in the previous studies of Willebrand et al. (2001) and Treguier et al. (2005) showed a strong sensitivity to the surface atmospheric forcing and numerical concepts used in the ocean models. The simulations in Willebrand et al. (2001) were forced with monthly mean climatological forcing. The convection depth of the five models was strikingly different—between 2,000 and 400 m.

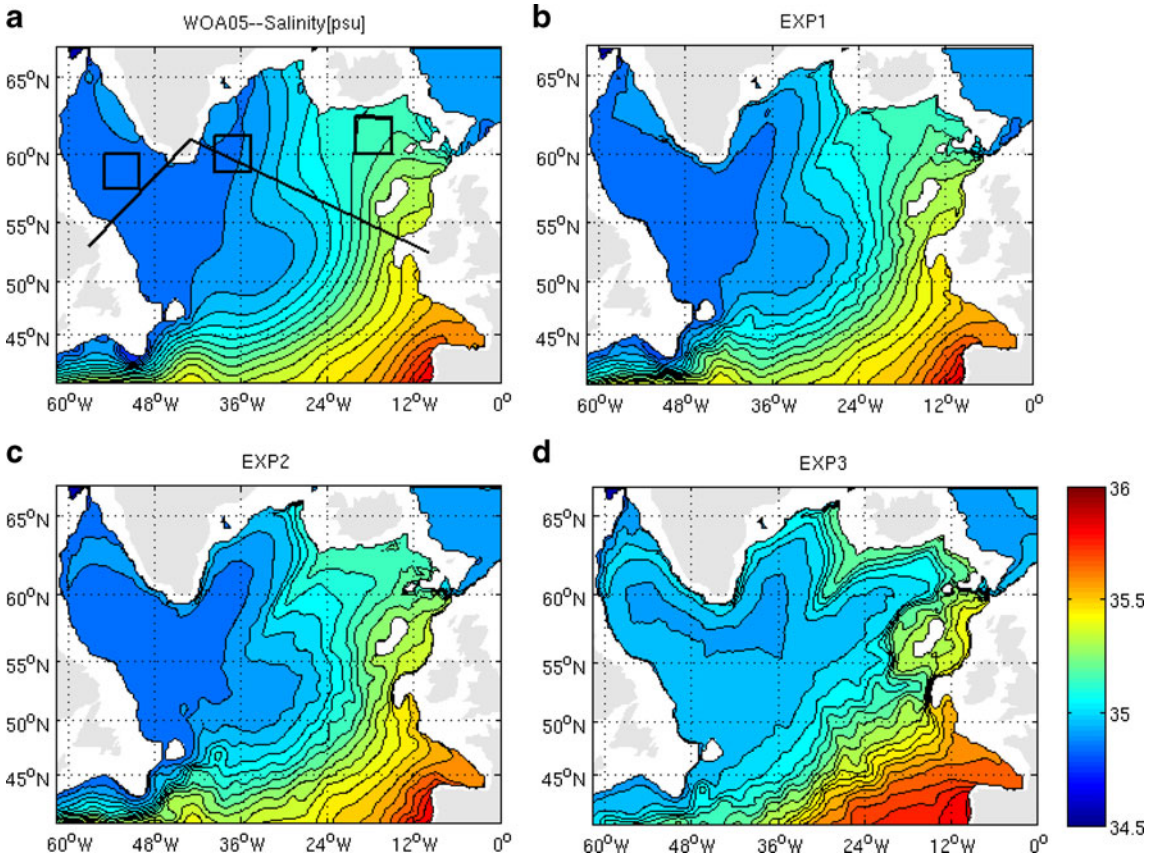

Fig. 6 As in Fig. 5 but for salinity. Contour interval is 0.05 psu. In **a**, the three *boxes* represent the regions where profiles will be extracted in Fig. 7, and along the sections *outlined in black* some results will be shown in Figs. 8d and 10d

The authors suggest that beyond the different numerical concepts "other factor can contribute" to the uncertainty in the model MLD and observe also "strong differences between realizations of the same model". The model MLD in Treguier et al. (2005) is simulated with four eddy-resolving ocean models. These authors find that the MLD is unrealistic and reaches the bottom in the experiments forced with interannual forcing (ATL6 and MICOM). It is not excessive and about 1,750 m in POPNA10 experiment and realistic in the FLAME experiment, both forced with climatological forcing (see Treguier et al. 2005). Here we try to assess how realistic is the MLD in the three model experiments. To do so, we compare them with the observed MLD.

The atmospheric fields used to force our simulations are monthly mean and those computed from the NCEP/NCAR reanalysis for the period (1968–1996). The existing observations (Yashayaev 2007) demonstrate that the depth of the deep convection in the Labrador Sea during this period varies between about 1,000 and 2,200 m. More specifically, Yashayaev (2007) describes this period in the following way:

(1) The Labrador Sea was warmer than usual (deep convection shallow and in some years even below 1,000 m) during the periods 1962–1971 and from 1977 to 1983. In 1970–1971, the Labrador Sea reached its warmest and saltiest state ever observed.
(2) The last warming started after 1994. It was seen through 2006 when the 150–2,000-m average temperature and salinity returned to the levels typical to the mid-1960s.
(3) The coldest period was from 1987 to 1994. This is the period when the winter convection reached highest depth for the whole period between 1968 and 2005. For the whole period from 1968 to 2006, there was only 1 year—1994—when the deep convection reached a depth close to 2,200 m.

The convection in the EXP3 experiment is excessive and reaches 2,500 m in most of the years. As mentioned before, the forcing of this convection is computed with monthly mean atmospheric climatology, which is not as strong as in the coldest years of early 1990s. The cause of the excessive deep convection in this experiment +is the warm and salty bias in the water column, which makes it additionally unstable. Finally, our interannual simulations with EXP2 setup discussed at the end of the present article closely follow the patterns (1)–(3) described by Yashayaev 2007.

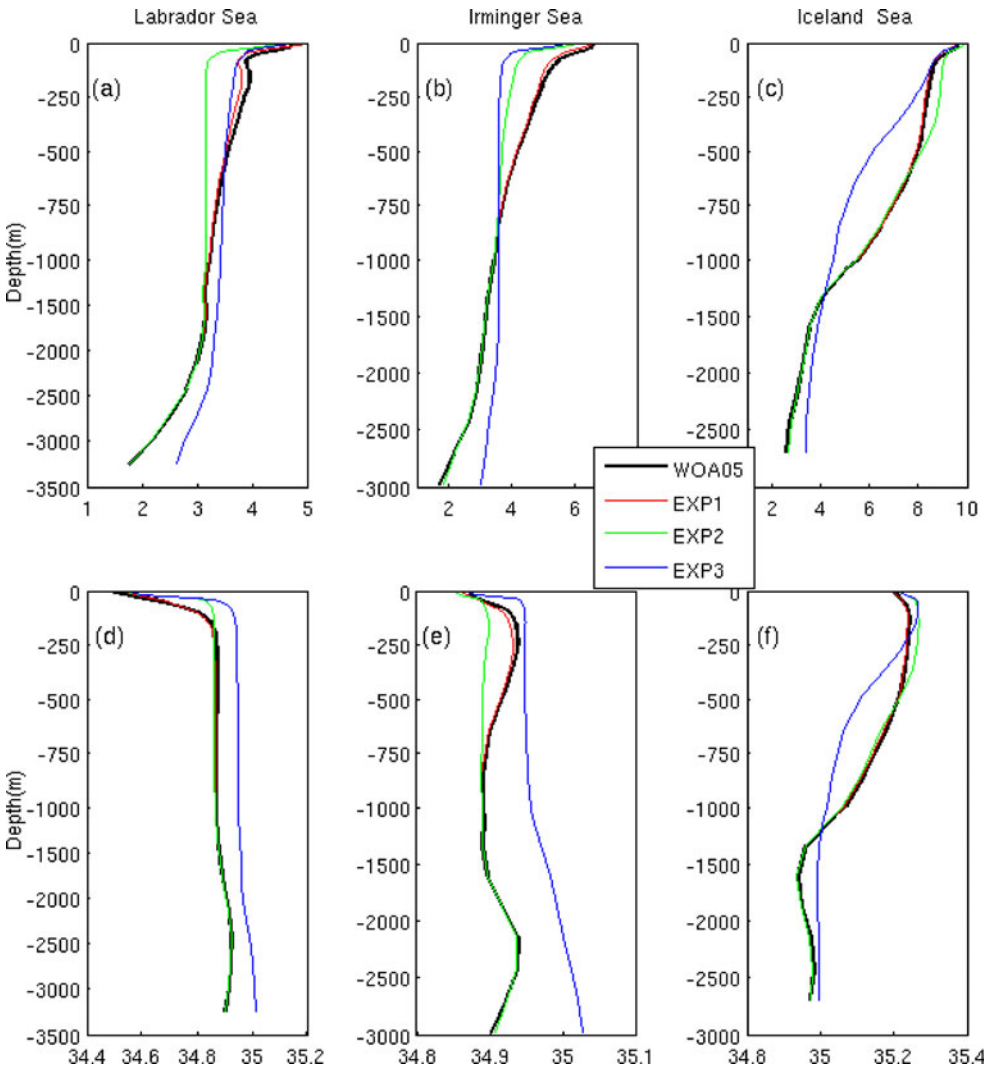

Fig. 7 Potential temperature (*upper*; unit: °C) and salinity (*below*; unit: psu) profiles averaged over three boxes defined in Fig. 6a, which refer to the inner Labrador Sea (**a**, **d**), the inner Irminger Sea (**b**, **e**), and Iceland Basin (**c**, **f**), respectively. The *curves* correspond to the climatologies of WOA05 and three experiments

Hence, the spectral nudging not only constrains the bias and excessive convection but is also a numerical concept that allows the realistic simulation of interannual variability in the MLD.

The three experiments, EXP1, EXP2, and EXP3, show significant differences in the spatial structure of the mixed layer and maximums of the MLD. The weakest deep convection is in the EXP1. While deep convection is driven by heat loss during the winter, the properties of the waters in the surface and intermediate waters formed during the previous years can play an important role for the preconditioning of the vertical mixing. The variability in these properties is suppressed by the spectral nudging in this experiment and does not allow the deep convection to develop as deep as in other experiments. In the EXP2, the MLD extends down to about 1,800 m. The salinity and temperature bias in the EXP3 has an impact on the vertical mixing and deep convection. Deep convection in this experiment is artificially intensified by increased salinity and temperature of the water masses and extends to the depth of about 2,200 m in most of the years. The position of deepest mixed layer in EXP3 is also unrealistic and too north-westward compared to observations.

4 Water mass transports

4.1 Barotropic streamfunction

Figure 9a–c shows the 5-year mean barotropic streamfunction (BSF) from EXP1, EXP2, and EXP3, respectively. EXP3 simulates the Gulf Stream separation unrealistically with the well-defined "Hatteras eddy". The later is related to a strong spurious recirculation in the region of Gulf Stream separation and is commonly observed in coarse resolution and eddy-permitting models of the North Atlantic (Willebrand et al. 2001). It is much weaker in EXP1 and EXP2 than in EXP3. Generally, EXP2 and EXP1 show a more similar pattern of BSF in the whole North Atlantic. In the Labrador and Irminger seas, they show an

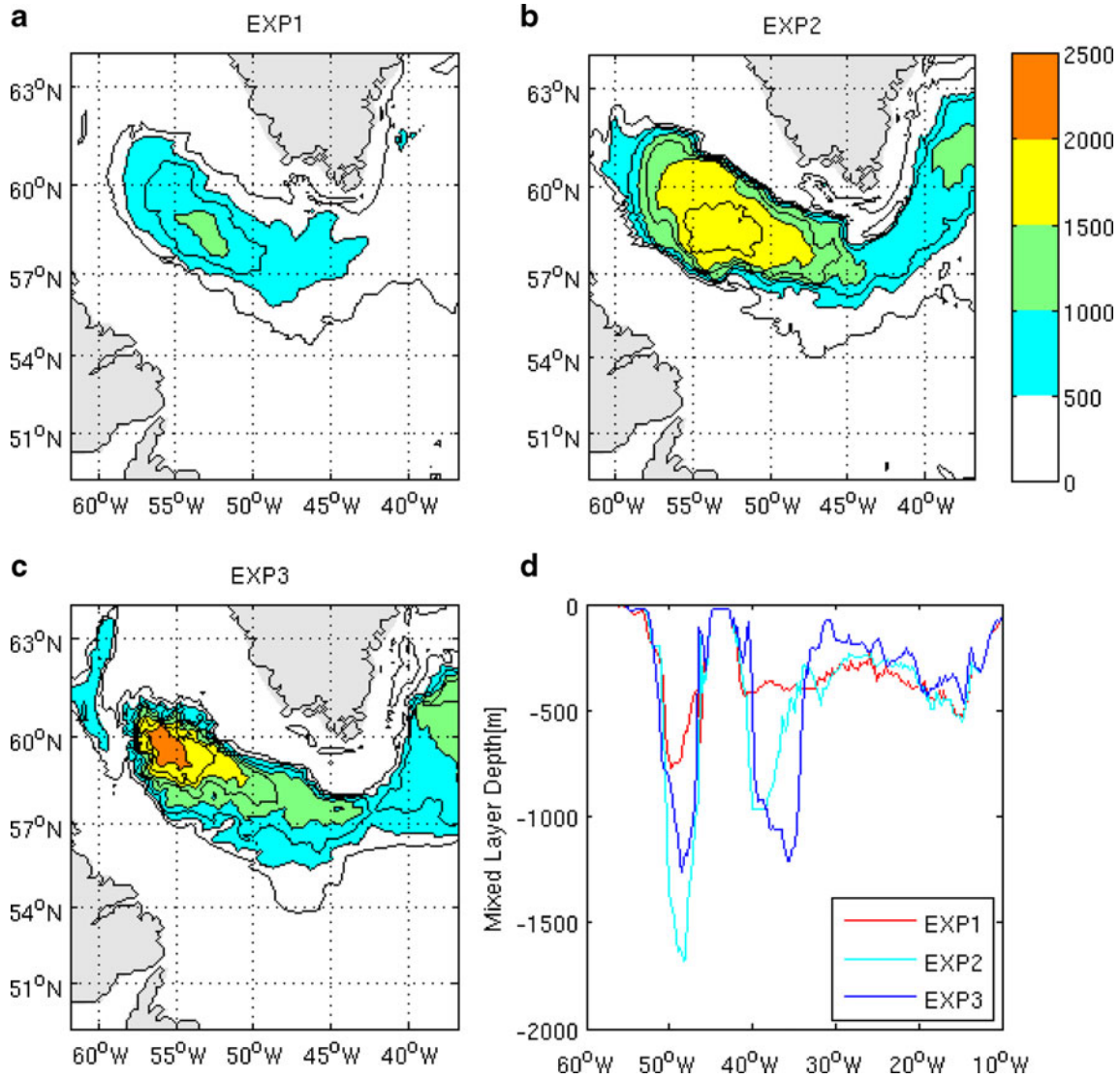

Fig. 8 Mixed layer depths (unit, meter) in the Labrador Sea at the end of March from **a** EXP1, **b** EXP2, and **c** EXP3. **d** Mixed layer depth at the end of March along the sections defined in Fig. 6a

improvement comparing to EXP3 and represent well the transport in the boundary currents and recirculations known from observations (Lavender et al. 2000). The experiments we have done (not shown here) demonstrated that the water transports and the elements of the circulation (i.e. recirculations) are improved significantly through a more realistic representation of the bottom topography by partial cell (also see Käse et al. 2001).

The barotropic streamfunction along the sections outlined in Fig. 6a is shown in Fig. 9d. The largest volume transport is observed in the Labrador Current system. In EXP1, this transport is about 44 Sv, which is close to the estimation of Pickart et al. (2002). The volume transport by the Labrador Current in EXP2 is a little larger, about 45 Sv, and EXP3 is close to 51 Sv. All three experiments simulate the partial recirculation eastward of the Labrador Current. In EXP3, it is about 11 Sv which is a little larger than the 10 Sv estimated by Pickart et al. (2002) from observations. In EXP1 and EXP2, this recirculation transport is much weaker, about 5 Sv, and is close to the estimation of Lavender et al. (2000). In this particular case, the observational studies do not provide accurate value of this transport and the difference between the volume transports in the three model simulations is within the uncertainty of the existing observational estimations. The model simulations in EXP1 and EXP2 suggest that there is a recirculation of about 5 Sv near the west Greenland Coast. It is not present in the EXP3.

In the Irminger Basin, all three experiments simulate the narrow area of intense volume transport in the East Greenland Current (about 45 Sv), which is in agreement with observational estimations farther downstream at Cape

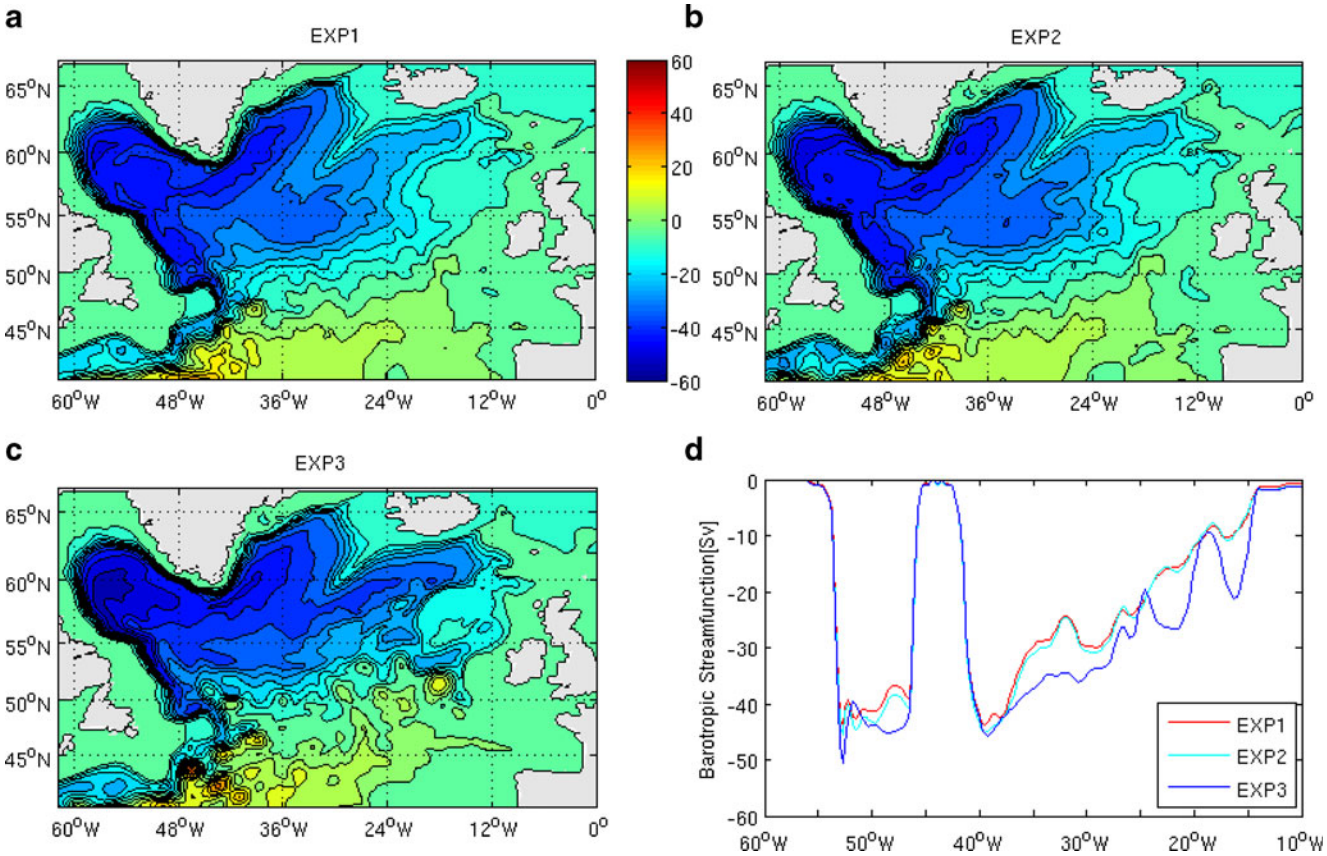

Fig. 9 The barotropic streamfunction (Sv) from **a** EXP1, **b** EXP2, and **c** EXP3, averaged over the last 5 years. Contour interval is 5 Sv. **d** The barotropic streamfunctions (unit, Sv) along the sections indicated in Fig. 6a

Farewell (30–50 Sv; Clarke 1984). The northward currents along the western flank of the Reykjanes Ridge is weaker in the EXP3 (about 11 Sv) than in the EXP1 and EXP2 with total transport of 20 Sv. Along the eastern flank of the Reykjanes Ridge, the simulated southward currents are all very weak, between 32° W and 30° W, about 5 Sv in EXP1 and EXP2 and less than 2 Sv in EXP3. The difference along the two sides of the Reykjanes Ridge between EXP3 and the other two experiments reflects the more southwards extension of cross-ridge flow in EXP1 and EXP2 (not shown here). Going eastwards further, EXP3 shows two well-organized recirculation cells, with amplitudes of about 10 Sv transports. In EXP1 and EXP2, there is no significant recirculation in this region.

4.2 Meridional overturning circulation

Figure 10a–c show the 5-years mean meridional overturning streamfunction for the North Atlantic in EXP1, EXP2, and EXP3, respectively. The overall patterns of the overturning streamfunction in EXP1 and EXP2 are similar but somewhat different from EXP3. The maximum transport in EXP1 and EXP2 is about 20 Sv, which is 2 Sv stronger than in EXP3. The maximum in EXP1 and EXP2 is in the region between 25° N and 45° N at a depth of about 1,000 m, while the maximum in EXP3 is positioned south of 20° N at the same depth as in the other two simulations. The volume transport of origin from the Nordic Seas which crosses the northern ridges and enters the subpolar North Atlantic is about 4 Sv. This value is close to the observed magnitude of flow (Dickson and Brown 1994). Due to the contribution of warm-to-cold conversion in the subpolar North Atlantic, the southward flow of the NADW increases significantly. The southward flow of the NADW is compensated by the northward flows in the surface 1,000 m and of the Antarctic Bottom Water. The transport of the Antarctic Bottom Water is weaker in the EXP3 than in EXP1 and EXP2.

4.3 Deep Labrador Current structure and transports

In this section, we compare the model simulations of the Deep Labrador Current and related volume transport with the observations of Dengler et al. (2006). These authors present the observational study of the Labrador Current from mooring data obtained along two sections across the shelf at about 53° N (hereinafter referred to as 53° N section; see Fig. 1) and 56° N (hereinafter 56° N section; see Fig. 1).

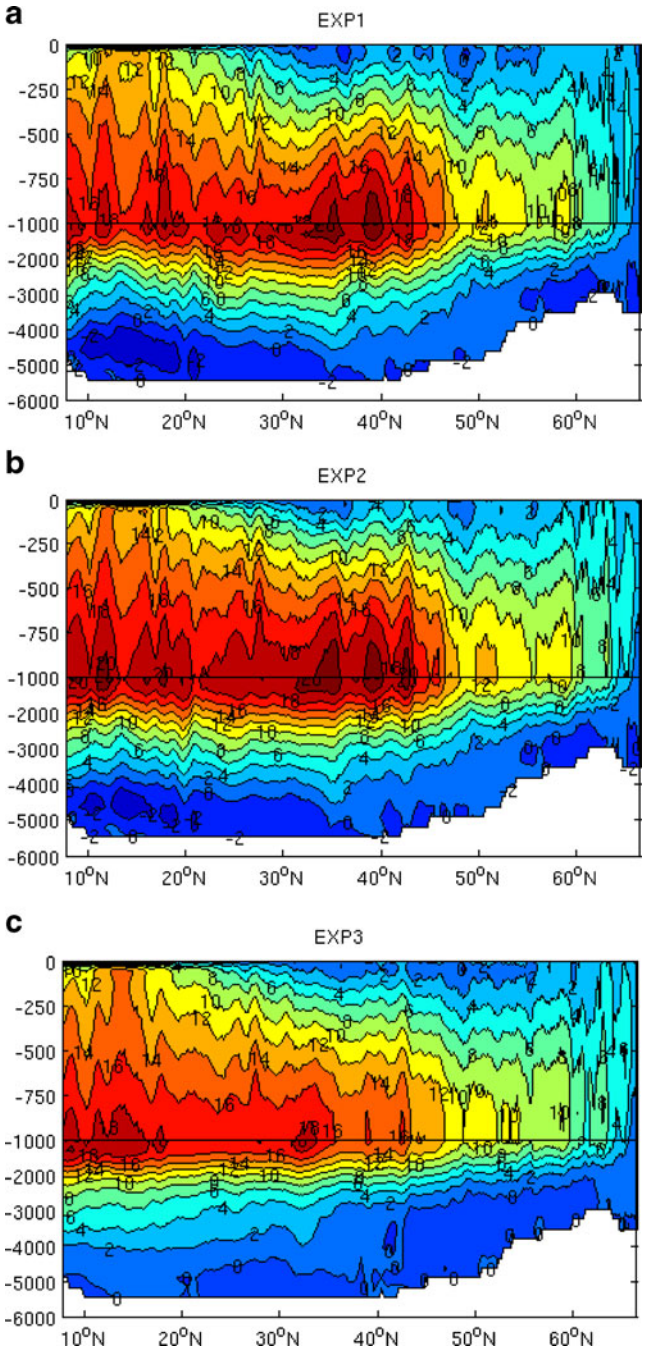

Fig. 10 The meridional overturning circulation streamfunction (Sv) from **a** EXP1, **b** EXP2, and **c** EXP3, averaged over the last 5 years. Contour interval is 2 Sv

Figure 11 shows the mean alongshore velocities from the three experiments. The velocity field along the two sections has a strong barotropic component and extends from the surface down to the bottom. Along 56° N section, the simulated Deep Labrador Current extends about 100 km offshore in the three experiments. This is a smaller than the 1996–2005 mean current extension of 120 km observed by Dengler et al. (2006). Offshore of the Labrador Current, the three simulations represent weak northwestward flows, which were mentioned above as counter-current recirculation (Lavender et al. 2000). The Labrador Current in the two experiments, EXP1 and EXP2, has similar intensities and extension. The Deep Labrador Current and the recirculation are in general broader and stronger in the EXP3 than in the two other experiments.

Along 53° N section, the simulated Deep Labrador Current extends from the shelf break to about 120 km offshore, which is also a little narrower than 140 km as estimated by Dengler et al. (2006) based on the 1996–2003 mean observational data. The simulated recirculation along this section is also stronger in EXP3 than in EXP1 and EXP2.

The volume transport calculated for different isopycnical layers along the 53° N and 56° N sections is shown in Table 2. The upper and lower boundaries of these layers are defined by the four isopycnal surfaces: σ_0=27.68, 27.74, 27.8, 27.88. The layers, 27.68≤σ0≤27.80, 27.80≤σ0≤27.88, σ0>27.88, are defined in a way to represent LSW, Gibbs Fracture Zone Water (GFZW), and Denmark Strait Overflow Water (DSOW), respectively (see Dengler et al., 2006). At 56° N, the total Deep Labrador Current transport in EXP1 and EXP2 are 31.6 and 32.9 Sv, respectively. These values are in a good agreement with the estimate of Dengler et al. (2006) which is 28.7±6.4 Sv. The transport in this layer in the EXP3 is unrealistically high and about 37 Sv. The transport of the two other water masses, LSW and GFZW, is 21.9 and 9.6 Sv in EXP1 and 23.4 and 9.4 Sv in EXP2, respectively. These values are close to the upper limit of the transport of the LSW and GFZW estimated by Dengler et al. (2006) which are 17.2±3.4 and −8.3±1.9 Sv, respectively. The LSW transport in the EXP3 is significantly higher than the observational values and is about 29.1 Sv. All three experiments underestimate the transport of the DSOW which is 0.1 Sv and much lower than the observed one—3.2–3.8 Sv. Within the recirculation, 12.9 Sv of deep water are re-circulated northeastward in EXP3, which is larger than those in EXP1 and EXP3 (7.0 and 7.8 Sv, respectively) by almost a factor of 2. Along the 53° N section, there is no big difference between the average Deep Labrador Current transports of EXP1, EXP2, and EXP3 (32.2, 32.6, and 32.6 Sv, respectively), which are also in good agreement with the estimates of Dengler et al. (2006) (31.0±4.7 Sv). However, transports within the recirculation of EXP3 (14.6 Sv) are much larger than in EXP1 (5.6 Sv), EXP2 (5.5 Sv), and observation (4.6± 4.1 Sv). In conclusion, EXP3 overestimates the volume transport for most of the water masses in the Western Labrador Sea. Myers and Deacu (2004) suggested in particular that the enhanced salty Atlantic Waters transport is one of the factors that contribute to the salinity bias of the water masses of the Labrador Sea.

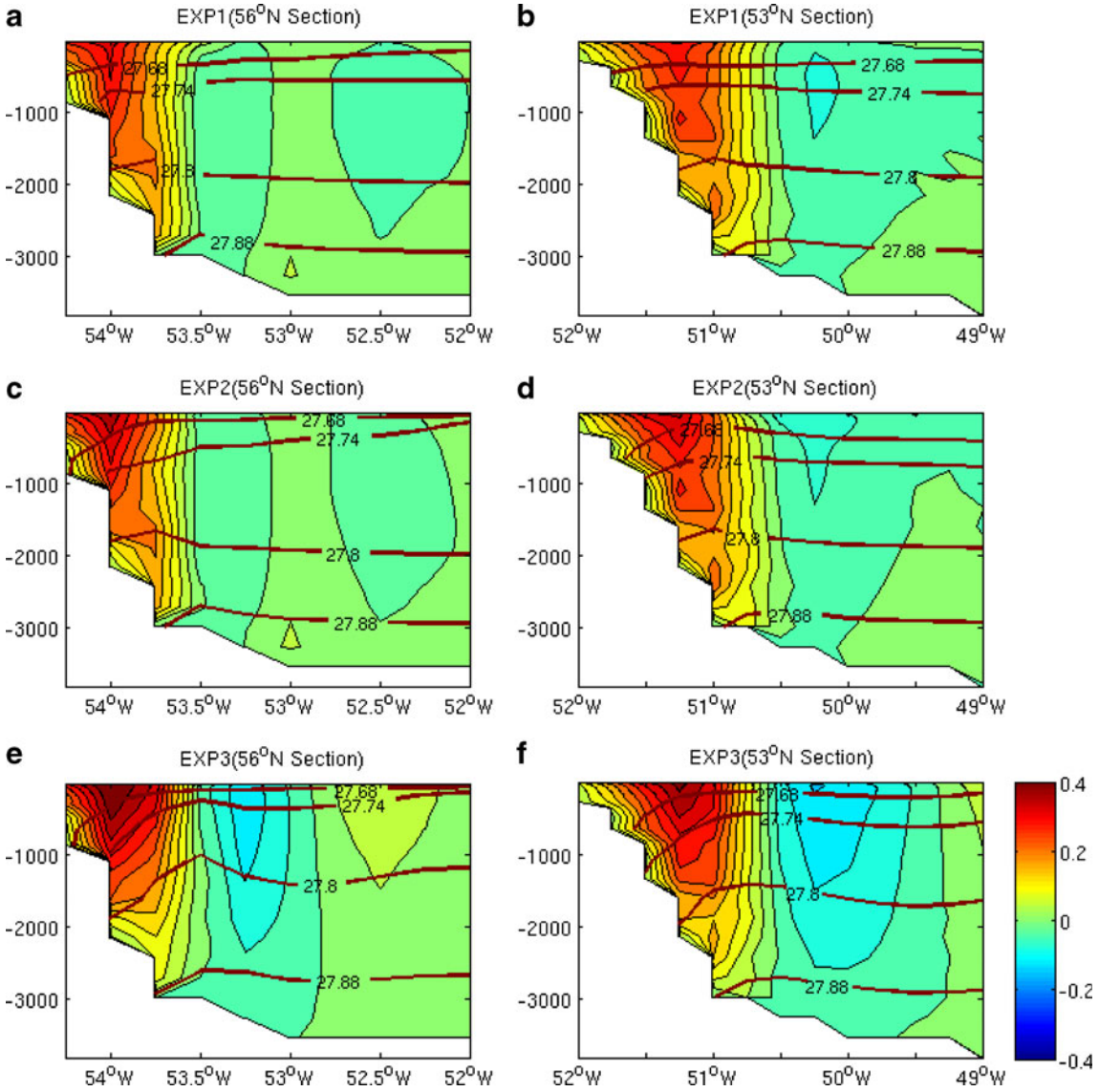

Fig. 11 Alongshore velocities for the 56° N (**a**–**c**) and 53° N (**d**–**f**) sections from EXP1 (**a**, **d**), EXP2 (**b**, **e**), and EXP3 (**c**, **f**). Contour interval is 0.04 m/s. The contours in *red* are potential densities with reference to surface

Table 2 The deep Labrador Current transports (unit, Sv) between isopycnal boundaries along 56° N and 53° N sections. Positive values indicate northwestward flow. In the estimations by Dengler et al. (2006), the transports along 56° N and 53° N sections are averaged over 1996–2005 and 1996–2003, respectively. The results are shown in the order of Estimations_by_Dengler et al., EXP1/EXP2/EXP3

	σ<27.68	σ=27.68~27.74	σ=27.74~27.8	σ=27.8~27.88	σ>27.88
56° N section	−6.3	−6.8 −17.2±3.4	−10.4	−8.3±1.9	−3.2±1.1
	−6.5/−5.9/−7.4	−7.0/−9.7/−13.9	14.9/−13.7/−15.2	−9.6/−9.4/ −7.8	−0.1/−0.1/−0.1
56° N section—recirculation	1.1	5.8±5.0		1.7±1.7	0.7±0.6
	0.4/0.3/0.7	0.7/0.9/1.5	3.7/4.2/5.6	2.0/2.1/4.8	0.6/0.6/1.0
53° N section	−6.3	−7.0 −18.3±2.9	−11.3	−8.9±1.8	−3.8±1.0
	−8.8/−9.0/−10.2	−6.4/−9.0/−11.7	−16.9/−14.9/−14.3	−8.6/−8.4/−6.5	−0.3/−0.3/−0.1
53° N section—recirculation	1.3	2.5±2.3		1.6±1.4/	0.5±0.4
	0.7/1.4/1.3	1.1/1.1/2.6	2.8/2.7/ 6.1	1.4/1.4/4.9	0.3/0.3/1.0

5 Conclusion and discussion

The temperature and salinity in the prognostic run EXP3 show a significant bias. Our results suggest that it is related to important changes in the major patterns of circulation. The model bias of temperature and salinity and the ocean circulation interact in a complex way and have an impact on the long-term prognostic simulations. The time variability of temperature, salinity, and kinetic energy on Fig. 2 shows that the strongest drift in these characteristics is observed in the first 5 years of the unconstrained EXP3 run from the 11th to the 15th year. The temperature and salinity in the sub-polar ocean at the end of the 15th year is warmed and saltier than in EXP1 and EXP2. The flow in the unconstrained run is stronger (Fig. 2a) than in the EXP1 and EXP2. The integral characteristics on Fig. 2 show the general tendencies in the model solution in the three experiments. At the same time, the model bias is not spatially homogeneous.

Figure 12 shows the spatial distribution of model drift in EXP3 at 60 m (Fig. 12a, b), 1,338 m (Fig. 12c, d) and 2,696 m (Fig. 12c). It is calculated as the linear trend in the difference of temperature and salinity in EXP3 and EXP1 between year 11 and year 15. The maximum in the model drift in EXP3 in the surface layer (Fig. 12a, b) of the sub-polar ocean is in the western part of the Labrador Sea and in the eastern part of the sub-polar gyre. The positive trend of temperature and salinity in the surface layer of the west Labrador Sea has a maximum along the coast of Labrador and Newfoundland. This is the region covered by sea ice

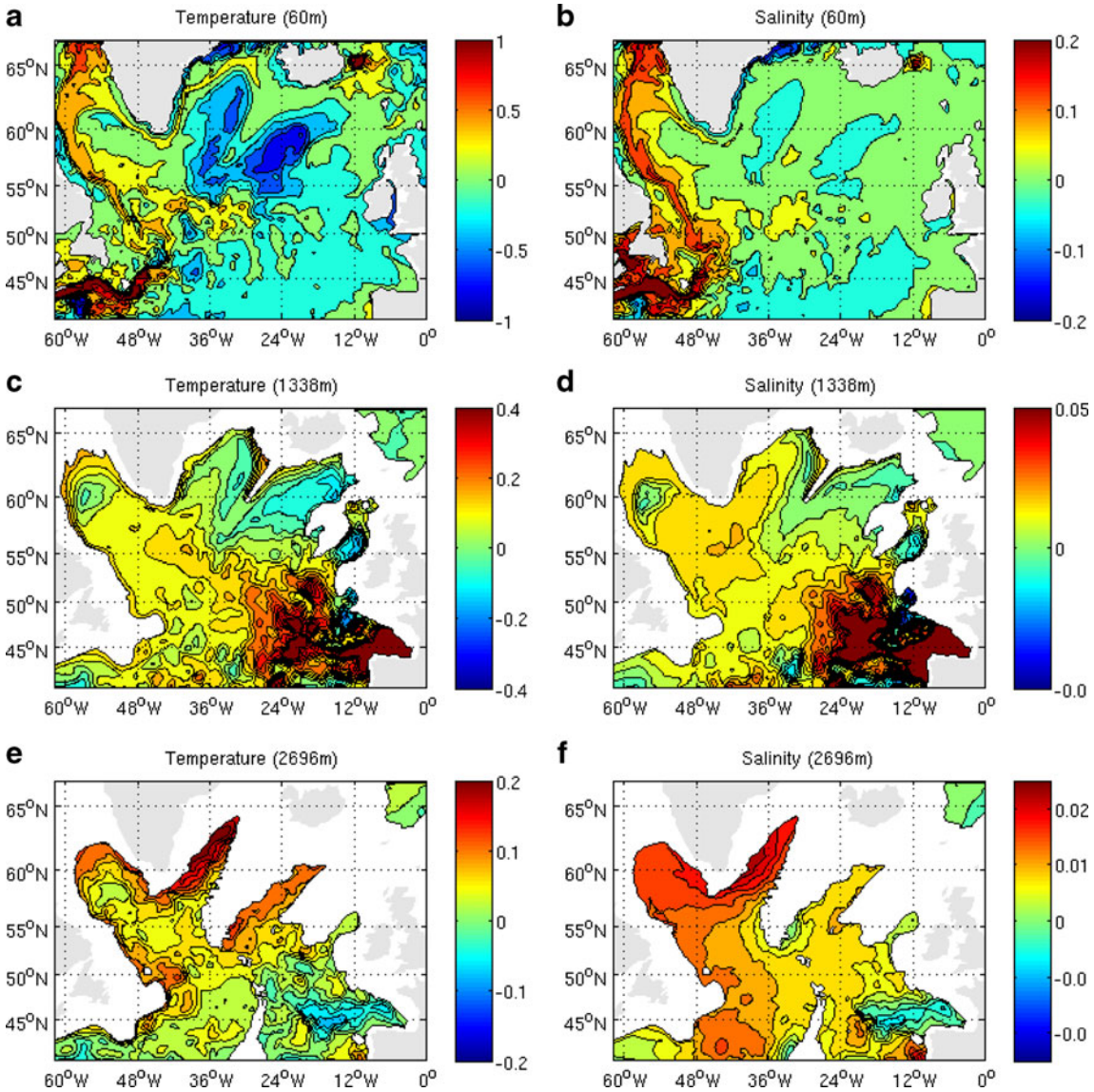

Fig. 12 The model drifts in EXP3 as shown by the linear trends from the model year 11 to year 15. **a**, **c**, **e** Potential temperature at 60, 1,338, and 2696 m, respectively (unit, °C/year). **b**, **d**, **f** Salinity at the same levels (unit, psu/year)

during the winter months. Cooke et al. (2010) demonstrated that the coupled ocean–sea ice model used in the present study underestimates the ice concentration along the coast of Labrador and Newfoundland. The sea ice variations are negatively correlated to the surface layer temperature and salinity (Deser et al. 2002). Hence, the positive trends in the temperature and salinity observed along the western coast of the Labrador Sea correlate well with the underestimation of the sea ice in the model simulations. The increase in the surface salinity driven by uncertainties in the surface water balance destabilizes the water column and leads to intensification of the winter convection (see Fig. 8) in EXP3. The intense vertical mixing in the central part of the Labrador Sea increases the cross-shelf slope of the isopycnical surfaces in EXP3 (see Fig. 11) which intensifies the sub-polar circulation (Figs. 9 and 11).

The convectively formed new waters at intermediate depths spread out of the Labrador Sea following the major pattern of the sub-polar circulation. Part the Labrador Sea Water LSW propagates towards the eastern part of the sub-polar gyre. In EXP3 the spreading LSW is saltier and warmer than in the other two experiments. This causes intensification of the horizontal density gradient at intermediate depths and additional intensification of the circulation in EXP3 in eastern sub-polar gyre. The intensified circulation impacts the temperature and salinity in the surface layer. The previous studies of Hátún et al. (2005) and Marsh et al. (2008) demonstrated that the surface layer temperature variability in this part of the North Atlantic depends on the strength and horizontal extension of the sub-polar gyre. When the sub-polar circulation is stronger than normal, the amount of the North Atlantic Current surface waters which penetrate into the eastern sub-polar gyre is smaller and temperature and salinity there are lower than normal. In EXP3, the horizontal circulation is stronger than in the other two experiments. Correspondingly, the temperature and salinity in the surface layer of the EPX3 is lower than in EXP1 and EXP2 (Fig. 12a, b). The model temperature and salinity bias at 1,338 m (Fig. 12c, d) is positive almost everywhere in the sub-polar gyre but in the areas of intense cyclonic flow in north Labrador Sea and eastern sub-polar gyre. The temperature and salinity bias in the deep layer is dominated by the effects of unresolved dynamical processes which govern the variability of the

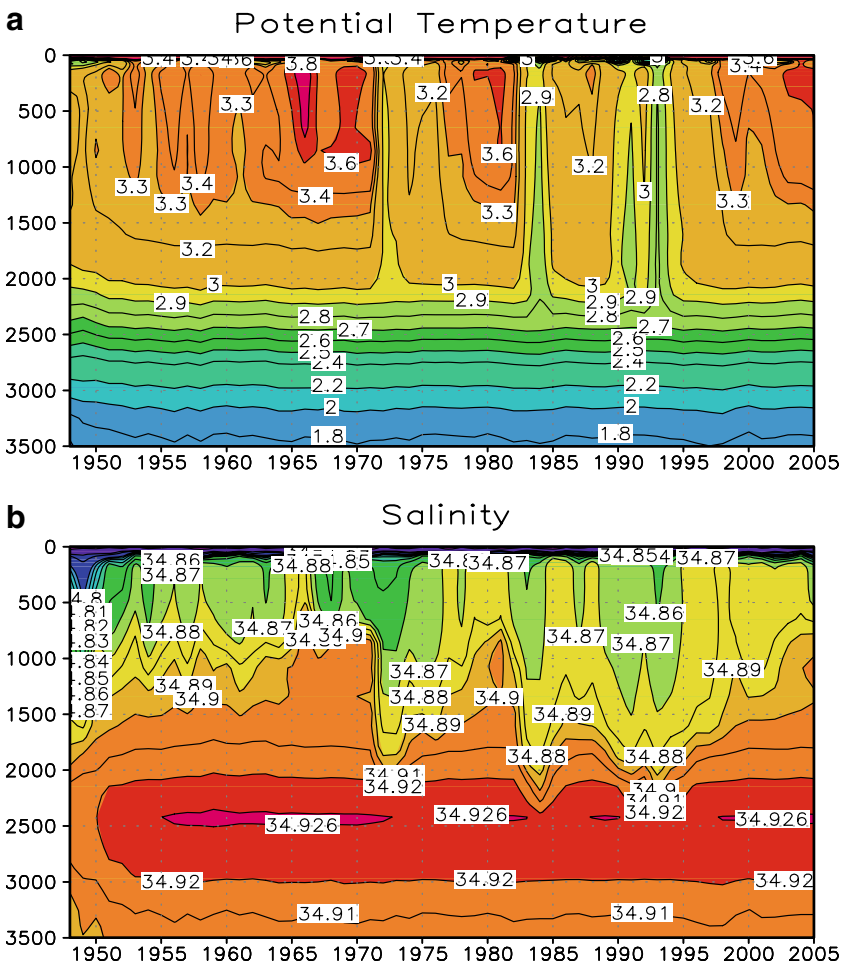

Fig. 13 Time series of the vertical distribution (from 0 to 3,500 m depth) of **a** potential temperature (unit, °C) and **b** salinity (unit, psu) in the central Labrador Sea during 1948–2005. The data are from an interannual run based on EXP2. The results are averaged for May–June of each year

overflows over the Greenland–Scotland Ridge. The deep-layer temperature and salinity in the unconstrained run EXP3 in the eastern sub-polar gyre are higher than in the other two experiments by about 0.2°C and 0.02 psu.

The results from the model simulations presented in this study demonstrate that the spectral nudging efficiently constrains the model bias. It suppresses the bias and allows the model solution freely to evolve in specified frequency intervals. The latter include the seasonal and mesoscale variability. In Zhu and Demirov (manuscript in revision), we study the skills of the present model setup to simulate the interannual variability in the Labrador Sea. Figure 13 shows the simulated potential temperature and salinity in the central Labrador Sea in this run. The model represents correctly the temporal patterns of the LSW variability in the past 50 years. The LSW was relatively warm/salty between late 1950s and early 1970s and turned cold/fresh between the late 1980s and mid-1990s. From 1987 to 1993, LSW became progressively cool and fresh due to a direct result of record deep and sustained winter convection that developed to its maximum depth at the end of this period. The trends of freshening and cooling reversed in 1994, and between 1994 and 2005 the upper and intermediate layers of the Labrador Sea steadily became warmer and saltier. This tendency was interrupted in 2000 with deep convection developing as deep as ~1,300 m. All these developments and subsequent evolution of LSW are consistent with the observational findings of Lazier et al. (2002) and Yashayaev (2007).

In this work, we used the spectral nudging method suggested by Thompson et al. (2006) to constrain the model bias. An alternative approach—the adiabatic semi-prognostic method for constrain of the model bias—was developed by Sheng et al. (2001) and Greatbatch et al. (2004). In the semi-prognostic method, the density in the hydrostatic equation is replaced by a linear combination of model-computed and climatological density. This procedure is equivalent to adding a forcing term to the horizontal momentum equation through a modification of the model's horizontal pressure gradient term.

Acknowledgments This work was funded by Canadian Foundation for Climate and Atmospheric Science through projects GOAPP and GR-631.

Appendix: The spectral nudging

Several factors contribute to the model drift, such as inadequate model resolution, poor parameterizations of sub-grid scale processes and inaccurate surface and lateral boundary conditions. In this study, we use the spectral nudging technique of Thompson et al. (2006) to suppress the model drift. This scheme corrects the model temperature and salinity in specific frequencies and wave-number intervals; outside these intervals the model is unconstrained.

Spectral nudging is implemented by adding a restoring term of the form $\lambda\langle X_t^{\mathrm{c}} - X_t^{\mathrm{f}}\rangle$ to the model's temperature and salinity update equations, where X_t^{c} is the observed climatology at time t and X_t^{f} is the corresponding model forecast. The restoring time is proportional to λ^{-1}. The angle brackets denote a filtered quantity that is close to zero for wave numbers above a specified cutoff and frequencies beyond κ of the climatological frequencies of zero and one cycle per year. For more details on the technique, see Thompson et al. (2006).

The spectral nudging corrections in regions of variable bottom topography can have a spurious effect on the barotropic mode. This effect is due to the inconsistency between coarse temperature and salinity climatology and strong slopes of bathymetry. It has the same form as the JEBAR effect (Mertz and Wright 1992; Greatbatch et al., 1991; Myers et al., 1996) and contributes to the bottom pressure torque. In this way, the spectral nudging can create spurious patterns in the circulation in areas of strong variations of bottom topography. To reduce this effect, the spectral nudging in EXP2 is applied at depths higher than 560 m. Additionally, a spatial filter is applied on the correcting term (see Thompson et al. 2006) which removes artificial strong gradients in the temperature and salinity corrections near the continental shelf.

References

Adcroft A, Hill C, Marshall J (1997) Representation of topography by shaved cells in a height coordinate ocean model. Mon Weather Rev 125:2293–2315

Arakawa A, Lamb VR (1981) A potential enstrophy and energy conserving scheme for the shallow water equations. Mon Weather Rev 109:18–36

Antonov JI, Locarnini RA, Boyer TP, Mishonov AV, Garcia HE (2006) In: Levitus S (ed) World ocean atlas 2005, volume 2: salinity. NOAA Atlas NESDIS 62, US Government Printing Office, Washington, DC, p 182

Barnier B et al (2006) Impact of partial steps and momentum advection schemes in a global ocean circulation model at eddy-permitting resolution. Ocean Dyn. doi:10.1007/s10236-006-0082-1

Blanke B, Delecluse P (1993) Low frequency variability of the tropical Atlantic Ocean simulated by a general circulation model with mixed layer physics. J Phys Oceanogr 23:1363–1388

Brankart J-M, Brasseur P (1998) The general circulation in the Mediterranean Sea: a climatological approach. J Mar Syst 18:41–70

Carton JA, Giese BS, Grodsky SA (2005) Sea level rise and the warming of the oceans in the SODA ocean reanalysis. J Geophys Res. doi:10.1029/2004JC002817

Clarke RA (1984) Transport through the Cape Farewell–Flemish Cap section. Rapp P-V Réun Cons Int Explor Mer 185:120–130

Cooke ME, Demirov E, Zhu J (2010) A model study of the mechanisms of interannual sea-ice variability in the Labrador Sea. J Geophys Res (submitted)

Dengler M, Fischer J, Schott FA, Zantopp R (2006) Deep Labrador Current and its variability in 1996–2005. Geophys Res Lett. doi:10.1029/2006GL026702

Deser C, Holland M, Reverdin G, Timlin M (2002) Decadal variations in Labrador Sea ice cover and North Atlantic sea surface temperatures. J of Geophys Res 107. doi:10.1029/2000JC000683

Dickson RR, Brown J (1994) The production of North Atlantic deep water: sources, rates, and pathways. J Geophys Res 99(C6):12,319–12,341

Dickson RR, Yashayaev I, Meincke J, Turrell W, Dye S, Holfort J (2002) Rapid freshening of the deep North Atlantic over the past four decades. Nature 416:832–837

Fichefet T, Morales Maqueda MA (1997) Sensitivity of a global sea ice model to the treatment of ice thermodynamics and dynamics. J Geophys Res 102:12,609–12,646

Gaspar P, Grégoris Y, Lefevre J-M (1990) A simple eddy kinetic energy model for simulations of the oceanic vertical mixing tests at Station Papa and long-term upper ocean study site. J Geophys Res 95:16179–16193

Greatbatch RJ, Fanning AF, Goulding AD, Levitus S (1991) A diagnosis of interpendatal circulation changes in the North Atlantic. J Geophys Res 96:22009–22023

Greatbatch RJ, Sheng J, Eden C, Tang L, Zhai X, Zhao J (2004) The semi-prognostic method. Continental Shelf Research, volume 24, issue 18. Recent developments in physical oceanographic modelling: part I. December 2004, pages 2149-2165, ISSN 0278-4343 (doi:10.1016/j.csr.2004.07.009)

Häkkinen S, Rhines PB (2004) Decline of the North Atlantic subpolar circulation in the 1990s. Science 304:555–559

Hátún H, Sandø AB, Drange H, Hansen B, Valdimarsson H (2005) Influence of the Atlantic subpolar gyre on the thermohaline circulation. Science 309:1841–1844

Kalnay E et al (1996) The NCEP/NCAR 40-year reanalysis project. Bull Am Meteorol Soc 77:437–472

Käse RH, Biastoch A, Stammer DB (2001) On the mid-depth circulation in the Labrador and Irminger seas. Geophys Res Lett 15:3433–3436

Lavender K, Davis RE, Owens WB (2000) Mid-depth recirculation observed in the interior Labrador and Irminger seas by direct velocity measurements. Nature 407:66–69

Lazier JRR, Hendry A, Clarke I, Yashayaev, Rhines P (2002) Convection and restratification in the Labrador Sea: 1990–2002. Deep Sea Res I 49:1819–1835

Locarnini RA, Mishonov AV, Antonov JI, Boyer TP, Garcia HE (2006) In: Levitus S (ed) World ocean atlas 2005, volume 1: temperature. NOAA Atlas NESDIS 61, US Government Printing Office, Washington, DC, p 182

Lohmann K, Drange H, Bentsen M (2009) A possible mechanism for the strong weakening of the North Atlantic subpolar gyre in the mid-1990s. Geophys Res Lett 36:L15602. doi:10.1029/2009GL039166

Liu Y, Thompson KR (2009) Predicting mesoscale variability of the North Atlantic using a physically motivated scheme for assimilating altimeter and Argo observations. Mon Weather Rev 137:2223–2237

Lu Y, Wright DG, Clarke RA (2006) Modelling deep seasonal temperature changes in the Labrador Sea. Geophys Res Lett 33: L23601. doi:10.1029/2006GL027692

Madec G (2008) NEMO reference manual, ocean dynamics component: NEMO-OPA. Preliminary version. Note du Pole de modélisation, Institut Pierre-Simon Laplace (IPSL), France, No. 27 ISSN, No. 1288–1619

Marchesiello P, Williams JM, Shchepetkin A (2001) Open boundary conditions for long-term integrations of regional oceanic models. Ocean Model 3:1–20

Marsh R, Josey SA, de Cuevas BA, Redbourn LJ, Quartly GD (2008) Mechanisms for recent warming of the North Atlantic: Insights gained with an eddy-permitting model, J Geophys Res 113, C04031. doi:10.1029/2007JC004096

Marshall J, Schott F (1999) Open-ocean convection: observations, theory, and models. Rev Geophys 37:1–64

Mertz G, Wright DG (1992) Interpretations of the JEBAR term. J Phys Oceanogr 22:301–305

Molines JM, Barnier B, Penduff T, Brodeau L, Treguier A, Theetten S, Madec G (2007) Definition of the interannual experiment ORCA025-G70, 1958-2004. LEGI report, LEGI-DRA-2-11-2006 (update September 2007)

Myers PG, Deacu D (2004) Labrador Sea freshwater content in a model with a partial cell topographic representation. Ocean Model 6:359–377

Myers PG, Fanning AF, Weaver AJ (1996) JEBAR, Bottom Pressure. Torque, and Gulf Stream Separation. Journal of Physical Oceanography 26:671–683

Penduff T, Le Sommer J, Barnier B, Tréguier A-M, Molines J-M, Madec G (2007) Influence of numerical schemes on current–topography interactions in 1/4° global ocean simulations. Ocean Sci 3:509–524

Pickart RS, Torres DJ, Clarke RA (2002) Hydrography of the Labrador Sea during active convection. J Phys Oceanogr 32:428–457

Stacey M, Shore J, Wright DG, Thompson KR (2006) Modelling events of sea-level variability using spectral nudging in an eddy-permitting model of the Northeast Pacific Ocean. J Geophys Res 111:C06037. doi:10.1029/2005JC003278

Sheng J, Greatbatch RJ, Wright DG (2001) Improving the utility of ocean circulation models through adjustment of the momentum balance. J Geophys Res 106(C8):16,711–16,728

Thompson KR, Wright DG, Lu Y, Demirov E (2006) A simple method for reducing seasonal bias and drift in eddy resolving ocean models. Ocean Model 14:122–138

Thompson KR, Ohashi K, Sheng J, Bobanovic J, Ou J (2007) Suppressing drift and bias of coastal circulation models through the assimilation of seasonal climatologies of temperature and salinity. Cont Shelf Res 27(9):1303–1316. doi:10.1016/j.csr.2006.10.011

Tréguier A, Barnier B, de Miranda A, Molines J, Grima N, Imbard M, Madec G, Messager C, Reynaud T, Michel S (2001) An eddy permitting model of the Atlantic circulation: evaluating open boundary conditions. J Geophys Res 106:22 115–22 129

Tréguier A-M, Theetten S, Chassignet E, Penduff T, Smith R, Talley L (2005) The North Atlantic subpolar gyre in four high resolution models. J Phys Oceanogr 35:757–774

US Department of Commerce, National Oceanic and Atmospheric Administration, National Geophysical Data Center (2006) 2-minute gridded global relief data (ETOPO2v2)

Willebrand J, Barnier B, Böning C, Dieterich C, Killworth P, Le Provost C, Jia Y, Molines JM, New AL (2001) Circulation characteristics in three eddy-permitting models of the North Atlantic. Prog Oceanogr 48:123–161

Wright DG, Thompson KR, Lu Y (2006) Assimilating long-term hydrographic information into an eddy-permitting model of the North Atlantic. J Geophys Res 111:C09022. doi:10.1029/2005JC003200

Yashayaev I (2007) Hydrographic changes in the Labrador Sea, 1960–2005. Prog Oceanogr 73(3–4):242–276. doi:10.1016/j.pocean.2007.04.015